Optical Techniques for Characterization of Distorted Liquid Crystal

Yu. A. Nastishin

Institute of Physical Optics, 23 Dragomanov str., Lviv 79005 Ukraine

Received 17.09.2001

Abstract

Optical characterization of a liquid crystal (LC) implies the identification of LC phases and reconstruction of the director distribution in a given LC specimen using optical facilities. Several techniques – Optical Polarization Microscopy (OPM), Polarization Confocal Microscopy (PCM), Magnetic Null technique, Crystal Rotation technique, Optical Conoscopy, RV-technique for the determination of nematic polar anchoring strength W are analyzed. The abilities of the techniques in the application to LC's are illustrated by the author's recent results obtained in collaboration with France and USA liquid crystal groups. Identification of new LC TGBA and lyotropic chromonic nematic phases via their defects, optical study of the interface between the lyotropic L_3 (sponge) phase and a solid substrate, computer simulation of the conoscopic patterns for distorted (including hidden deformations) nematic LC cells and their experimental observations, protocol for the measurements of W, the RV-technique and other results are among the problems solved using optical techniques analyzed in this paper.

Keywords: liquid crystals, nematic anchoring energy, defects, conoscopy

PACS: 42.25.Lc, 42.30.Sy, 42.70.Df

Outline

1. Introduction

The characterization of a liquid crystal (LC) consists in obtaining the information on the structure and physical properties of a LC specimen. This examination procedure might follow one of purposes: to find a new material with desired properties, to measure material or LC cell parameters necessary for further study or application or to reject a LC cell that does not fit the technological requirements. Generally the technique is applicable for the characterization if it is nondestructive and unambiguously conclusive. Applying to the LCs most of optical techniques meet the case. A reader can find the information on physical properties of LCs in the

books [1,2]. The aim of this paper is to represent our recent results which demonstrate the ability of classical optical techniques to solve new problems as well as to introduce new optical characterization techniques developed with the author's participation. The results presented below were obtained in collaboration with O.D.Lavrentovich, S.V.Shiyanovskii, R.D.Polak - Liquid Crystal Institute, KSU, Kent, Ohio, USA; M.Kleman (Laboratoire Mineralogie-Cristallographie, Universite Pierre et Marie Curie, Paris), J.Malthete (Institute Curie, Paris); T.Nguyen (Centre de recherche Paul Pascal, Pessac, France); O.B.Dovgyi, O.G.Vlokh (Institute of Physical Optics, Lviv, Ukraine).

For any new material suspected to exhibit a LC state the characterization begins from the identification of LC phases. The identification techniques test the specific distinctive properties of the phase. Studying the optical properties of a specimen or its optical response to an external action in most cases one can unambiguously identify the LC state. Amongst the characterization techniques the most attractive are techniques which bring the information in a visual form accessible for direct eye analysis. There are several techniques designed for this aim. Amongst them the ***polarization microscopy (PM)*** traditionally plays a special essential role. To illustrate this statement one can recall that the LC phase as a new state of matter was discovered using the polarization microscope.

Polarization microscopy (PM). This technique is based on the property of LC to visualizes its internal structure via specific textures produced by polarized light passed through a sample with distorted director field and analyzer [3-5]. Most of LC phases exhibit a characteristic textures which unambiguously distinguish this phase from other LC phases. To a recent days a Twist Grain Boundary Phase (TGB) was an exceptional example of a LC phase that could not be identified by the polarization microscopy. In the first part of the talk I shall report on optical observations of nontrivial pretransitional phenomena evidenced by defects transformations at the cholesteric (N*) $\leftrightarrow$ smectic A (SmA) transition in cholesteryl nonanoate (CN). We have shown that cholesteryl nonanoate, a thermotropic compound which is well known to exhibit pretransitional effects at the smectic A (SmA) cholesteric (N*) transition [6,7], has in fact a TGBA phase in-between. Our arguments rely on the observation of new TGBA defects, either in Robinson spherulites cooled from the N* phase or in free standing films. The same new defects can be obtained in a well documented TGBA phase of a tolane compound.

Liquid crystals in general exhibit quite reach phase diagram. Besides the bulk phase transitions there is a special type of the phase transitions, so called *anchoring transitions.* At the anchoring transition the LC crystal remains in the same phase state, while its orientation spontaneously changes at some temperature point T_a. The order parameter that changes in the point T_a is the angle between the director and substrate (pretilt angle). The transition is driven by temperature. In 3-rd section of this talk I shall demonstrate how the anchoring transition can be visualized by defects transformations observed under the polarization microscope.

As long as the information on the phase diagram of a given material is available a LC cell with desired alignment and geometrical configuration can be prepared for further study or application. The desired alignment of the director in a LC cell can be achieved following one of alignment procedures described in literature. Review of the alignment techniques can be found in [8,9]. In practice the configuration of the director field in some fabricated cells might deviate from the expected structure even if all the precautions required by the technology of the alignment procedures seems to be followed. Any newly prepared cell must be characterized. First of all one has to examine the texture of the cell under the polarization microscope. However a PM yields

only a two-dimensional information, integrating the three-dimensional pattern of optical birefringence over the path of light. Singular defects and in-plane distortions produce special textures under the polarization microscopy, while continuous out-of-plane distortions cannot be detected by the polarization microscopy. Further let us call these distortions *hidden deformations*. The techniques for the characterization of hidden deformations in LCs are in great demand. At present an universal receipt to detect hidden deformations is not available. In most practical cases the experimenters disregard possible hidden deformations hoping that the exact maintenance of the cell preparation procedures guarantees expected alignment. However there is a risk of uncontrolled deviations from the technology for some particular cells. These cells must be recognized and rejected. Each type of suspected hidden deformation has to be studied in a special way. The problem of hidden deformations characterization can be solved by Confocal Polarization Microscopy (CPM) [10].

Fluorescence Confocal Polarizing Microscopy (FCPM). The FCPM is the version of the confocal microscopy (CM) [11] in which the medium under examination is doped with a fluorescent probe and the observation is performed in polarized light [10]. Initially the CM was designed for increasing the contrast of microscope images, particularly in thick specimens [12]. In the CM the observed volume is restricted by special optical design: the point light source and the inspected region (voxel) are confocal; light coming from the neighborhood of the inspected region is blocked by a pinhole. To obtain the three-dimensional (3D) image the specimen is gradually scanned in horizontal planes voxel by voxel by the focused laser beam. The resulting image is a stack of thin (submicron) horizontal optical slices. Whole data is stored in a computer as a 3D matrix of light intensity values recorded from each studied voxel. A vertical crossection of the specimen image can be plotted by special software as a two-dimensional matrix of the points of different brightness (or color) recalling the corresponding information from the computer memory. In the fluorescence confocal microscopy (FCM) the inspected specimen is doped by a high-quantum-yield fluorescent dye that strongly absorbs at the wavelength of the exciting laser. Exited dye molecules fluoresce at somewhat longer wavelength, defined by so called Stokes shift. For essentially large Stokes shift the exciting and fluorescence light signals can be separated. The intensity of the fluorescence light that reaches the detector is recorded by the computer. If the specimen is heterogeneous, the concentration of the dye dopant is coordinate-dependent. The resulting image has the contrast that is much higher than without the dye. It makes possible to visualize features in living cells and tissues; as well as to study coarse-grained phases and patterns. It was demonstrated in [11] that by adding a feature of polarized light observation, one can expand the capabilities of the FCM to visualize the director patterns in LCs. The FCPM technique has been recently used to visualize 3D director distortions in the field-induced Frederiks transition in the nematic LC and complex distortions associated with the focal conic domains in the smectic A. Earlier applications of FCPM represented some 3D structures in cholesterics. The resolution of the FCPM is still an open question. However the experiment shows that the resolution of the FCPM is worse in comparison with FCM [11]. When the sample is birefringent the light wave is split into eigenwaves which in general propagate with different refractive indices and as a result the light beam spreads; the image blurs and its contrast worsens. Although FCPM is a perspective characterization technique, it cannot yet be widely used: it is complicate, expensive and is available not in many laboratories.

Optical conoscopy. Some hidden deformations can be detected and characterized

by optical conoscopy. We have proposed an alternative approach for the analysis of the conoscopic patterns via computer simulations [13]. At the computer simulations the conoscopic pattern is plotted using complete expressions describing the light propagation in the crystal, while the traditional analysis procedure requires approximate reducing of the original equation for the phase retardation to an equation of the second order curves. The simulated conoscopic patterns contain all the details of the experimentally observed conoscopic figures including their fine structure, and demonstrate the validity of the proposed algorithm. The application of optical conoscopy for the detection of hidden deformations will be discussed in the section 5.

If the LC cell structure is known the material constants describing bulk properties of a given LC phase as well as surface parameters characterizing the interaction of the LC with the substrate can be measured. Using optical techniques one can measure several material parameters including Frank's elastic constants. In fact the techniques for the measurements of bulk material constant became classic and are used by the experimenters without modifications, while the methods for the characterization of the surface parameters (alignment state, pretilt angle, anchoring energy coefficients, surface order parameter) mostly were proposed in a recent years and are still in progress.

One of the parameters needed at commercial applications, particularly for LC display technology is the pretilt angle. The pretilt angle is the angle of the director at the surface measured from the plane of the substrate with no applied field. Two techniques: Crystal Rotation Technique (CRT) [14] and Magnetic Null Technique (MNT) [15] can be used to measure the director pretilt angle.

CRT. To measure the pretilt angle by CRT one has to orient the cell with its optic axis being at 45^o with respect to the incident light polarization direction and rotate it between crossed polarizers around the in-plane line which is parallel to the polarizer direction. The recorded light transmittance is a periodical function of the light incident angle and is symmetrical with respect to the angle related to the pretilt angle. From the value of the angle corresponding to the symmetry point one can calculate the pretilt angle value taking into account the Snell's law. In fact CRT is nothing else but the conoscopy performed for one azimuth of incidence plane with respect to the incident light polarization. However CRT technique can not be applied to the cells with hidden deformations.

MNT. To measure the pretilt angle by MNT an uniformly oriented liquid crystal cell is placed in the magnetic field. The zero angle ($\theta = 0^o$) of the orientation of the cell corresponds to the position when the perpendicular to the substrates is parallel to the magnetic field direction. A magnetic field is applied to a cell to deform the liquid crystal director within the cell. The deformation is detected by looking for changes in the optical transmittance of the cell between the crossed polarizers. The cell will be not distorted by the magnetic field if the director is parallel to the magnetic field. Gradually changing the angular position of the cell with respect to the magnetic field direction one find the angle of the cell orientation $\theta = \theta_p$ at which magnetic field does not change the light transmittance. The measured θ_p value is equal to the value of the pretilt angle. If there is no angular position of the cell at which the magnetic field does not changes the transmittance of the cell then the director field is distorted in the plane perpendicular to the substrates. Other techniques have to be used to characterize hidden distortions.

Optical techniques for the determination of the anchoring coefficient. This parameter also termed as anchoring strength is important for practical applications. The anchoring

coefficient represents a work needed to reorient the director from the easy axis [16, 2]. The easy axis is the equilibrium orientation set by anisotropic molecular interactions at the surface in the absence of any external fields. An external field can deviate the director from the easy axis. Experimental determination of the anchoring strength is of prime importance in understanding the surface phenomena in liquid crystals. There are numerous techniques to achieve the goal [17-37]. ***Testing techniques*** deduce the anchoring strength from the characterization of surface-stabilized wall defects [18,19], distorted director field in wedge cells [20], or from light scattering at the surface fluctuations [21]. ***External-field techniques*** [22-37] measure director deviations as the function of the applied field. The field techniques use dielectric or diamagnetic Frederiks effects in intermediate or high fields, as well as polar effects of flexoelectric and surface polarization origin. The most popular ***'high-electric-field' technique*** [28-37] to determine the polar anchoring coefficient W of a nematic-substrate interface requires the simultaneous measurement of the capacitance and optical phase retardation of a liquid crystal cell as a function of applied voltage. We develop a generalized model that makes it possible to eliminate the capacitance measurement. The new technique, called the ***RV (retardation vs. voltage) technique*** [31], requires only the measurement of retardation as a function of applied voltage, and allows for the determination of W by a linear fit over a prescribed voltage window. The technique is not sensitive to uniformity of the cell thickness, does not require patterned electrodes, and allows for the local probe of the surface.

Characterization of absorbing LC's. It is known that the optics of absorbing crystal is much complicated than it is for the transparent crystals [38, 39]. For this reason not many papers in current literature are devoted to the methodology of optical characterization applying to LCs. The validity of optical characterization techniques designed for transparent LCs in application to the absorbing LCs is not evident. One can find in literature the optical characterization techniques for solid absorbing crystals. Its application to the absorbing LCs needs special consideration and is still an open question. In the last part of this talk I represent some results demonstrating how the solid crystal characterization procedure can be adopted for chromonic nematic liquid crystals.

2. Identification of a TGB phase via its defects

This work was performed in collaboration with M.Kleman, J.Malthete and T.Nguyen and partially was published in [40]. Light microscopy of textures and defects have always played an essential role in the discovery of the physical properties of liquid crystals (LC) and remain a most easy and powerful tool for their characterization. The textural study of LC's gives a direct information on the structure of a studied phase. TGBA's have been under study for 10 years already, but yet little investigated for the nature of their defects. The situation with the investigations of these phases is not typical for LC's. As a rule the study of new LC phase starts from its textural characterization. However the typical textures of a TGBA phase containing large number of defects are very similar to the cholesteric textures. The solution of the problem is to prepare the isolated defects and follow their transformations during the phase transitions. For this purpose we studied defects transformations in freely suspended droplets and free standing films for four different compounds: cholesteryl pelargonate (CN), cholesteryl myristate (CT), T10 (see [41] for the reference) and chiralized 8CB.

CT, and 8CB doped with CT, exhibit a first order N* ↔ SmA transition. On the other hand, CN is considered as a standard example of a *weakly* first order N* ↔ SmA transition, and some effort has been done at a time to

investigate pretransitional effects in this compound (X-ray scattering measurements of the smectic order parameter [6], pitch and elastic constants divergence [42- 44], etc.). The smectic order parameter is a complex number, and both McMillan [7] and de Gennes [45] noticed the analogy with the normal metal ↔ superconductor transition.

The TGBA phase is in fact an analog of the Abrikosov phase. Let us remind that the structure of the TGBA phase consists of SmA slabs of finite constant size, rotated one with respect to another by a finite constant angle, about an helical axis (χ axis), parallel to the smectic layers. The boundary between adjacent slabs is a twist grain boundary (TGB) made of parallel equidistant screw dislocations of the SmA phase, which we can term *vortex* lines, in reason of the analogy with vortices in superconductors. This model is due to Renn and Lubensky [46], prior to any experiment. It has been successfully documented in several materials, on the basis of X-ray scattering, light selective reflection and freeze-fracture observations [47-50, 41]. In addition, a new phase, NL*, described as a TGBA phase with melted (liquid-like) vortex lines has been proposed [51]. The phase sequence N* ↔ NL* ↔ TGBA has been observed in T10, see [41]. TGBA textures have been little investigated yet, except [50] in a Grandjean wedge geometry.

The freely suspended droplets were prepared in 400 μm thick flat capillaries (Vitrodynamics) by mixing a powder with glycerol. Far away from the N* ↔ SmA transition the N* droplets of CN, CT and T10 have the structure of Robinson spherulites [52] with a disclination radius of strength $k = 2$ (4π rotation of the cholesteric local trihedron of directors about the disclination [53]) extending from the boundary of the droplet to a terminal point in the center of the droplet (N* defects of strength $k = 2$ can escape to a zero defect [54]). The droplets display a Maltese cross between crossed polarizers – four black brushes crossing at the center of the droplet. This texture is characteristic of spherical cholesteric layers when the anchoring conditions are planar [55]. The droplets texture does not depend on their size, except for very large droplets flattened between two surfaces, which are outside the present investigation. The CT droplets texture does not change upon cooling down to the transition to SmA. In CN, at $T_1 = T_c + 1°C$, and in T10, at T= 105.8°C (where the NL* phase is expected), the central terminal point of the defect splits into a planar, slightly anisometric, loop, Fig. 1a attached to the disclination radius. The region inside the loop has a uniform color, due to a selective reflection from the helical structure, when the plane of the loop is perpendicular to the microscope axis. This

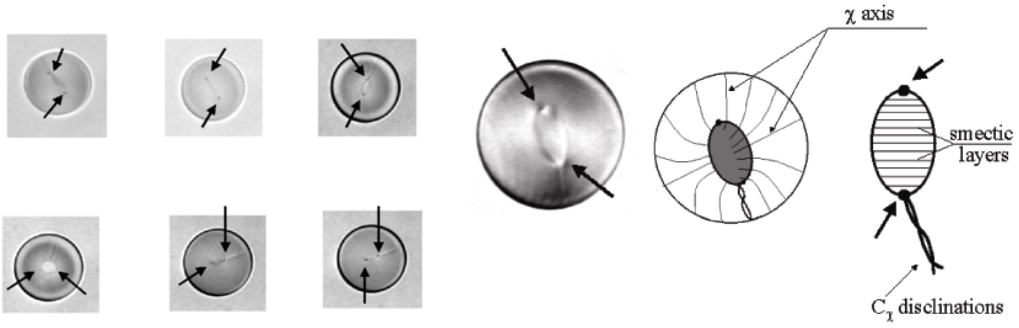

Fig. 1 Loop defect in a TGBA droplet of CN: a) different orientation of the loop for the same droplet in different temperature cycle, b) schematical representation of the structure of loop defect.

indicates that the director orientation is uniform in this plane. The diameter of the loop scales approximately as the size of the droplet and can be much larger than the pitch. The loop size is stable as long as temperature is constant, and increases as temperature is lowered. There are two diametrically located point defects on the loop (shown by arrows in Fig. 1a). They are poorly visible when the loop plane is perpendicular to the microscope axis, and better contrasted when it is parallel to the microscope axis. They scatter light, being visible without polarizer and analyzer. Their position does not move along the loop under defocusing. Such features imply that these points are singular point defects. We believe that these two points mark the termination of the parallel smectic layers in the plane of the loop (Fig. 1b). Near the phase transition it is observed that the disclination radius is split into two defect lines wound into a double helix and connected by the loop in the central region of the droplet. The diameter of the loop increases by mechanical rotation of the structure of the droplet around the line defect, whose effect is to unwind the double helix. As a result the plane of the loop has a random orientation with respect to the plane of the capillary limiting surfaces (Fig. 1a). Although we observed that on cooling in the T10 droplets the diameter of the loop increases much quicker as temperature passes through the value T=103.1°C, where according to [41, 49] the NL* $\rightarrow$ TGBA phase transition is expected, we were not able to identify this temperature point unambiguously. The texture transformations are reversible in temperature and can be followed on heating. We conclude that Fig. 1a shows a texture characteristic of the TGBA phase. This conclusion is supported by the fact that this texture does not appear for CT and CT+8CB droplets, and was never reported for N*. in the absence of the TGB phase between the cholesteric and the smectic A phases (which is the case of chiralized 8CB) the size of the central region is of order of the pitch and no loop is observed.

Free Standing films. Fig. 2 shows defects observed in *free standing films*, prepared inside 42 μm × 42 μm squared holes of standard electron microscopy copper grids, a technique recently used for nematic thin films [56]. The thickness of the films is estimated ≅ 5μm. Starting from the SmA phase of CN and increasing temperature, one grows a regular texture with the χ axis in the plane of the film, almost everywhere perpendicular to the nearest edge of the limiting square, Fig.2. Such an alignment of the χ axis produces four diagonal tilt grain boundaries of the slabs and a $k = 1$ line singularity of the χ director in the center of the square. This singularity splits into two singular lines k=1/2 from which two spirals extend through the sample. The same texture was obtained for T10 below T=103°C, where a TGBA phase is expected. Additional new defects appear upon heating, at T_1, the TGBA $\rightarrow$ NL* phase transition. In both cases, viz. CN and T10 films, the film uniform color observed between crossed polars shows that the direction of the film thickness averaged optical axis i.e. the χ axis, is strictly in the plane of the film and strongly oriented.

A further evidence - that the local order of CN below T_1 and the local order of chiralized 8CB indeed differ - follows from the flickering

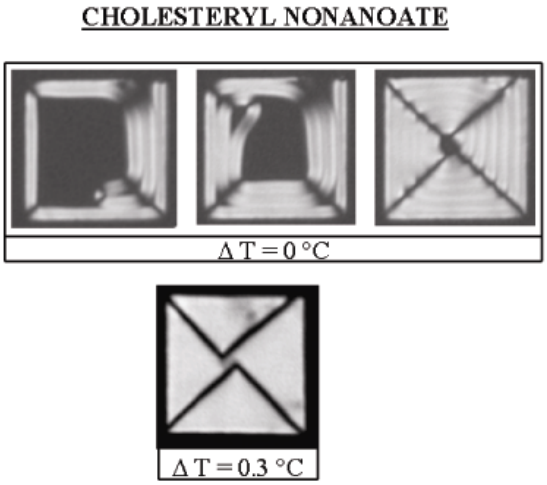

Fig. 2 Textures of free standing films.

of the director observed for chiralized 8CB but not for CN and T10: the thermal fluctuations of the nematic director produces a scintillating contrast of the texture between crossed polarizers for chiralized 8CB; the CN and T10 textures do not have such a feature.

3. Anchoring transition visualized by defects transformations

The LC interface exhibits a reach variety of behaviors: surface ordering [57-62], surface melting [63], degeneration of the azimuthal director orientation [1,64-67], memory effects [68], temperature driven, field or light induced anchoring transition [69-82], orientational wetting [57,83-85] and spreading [86,87], spontaneous generation of periodical distortions and defects with nontrivial topological charges [66, 67], surface polarization [88], etc.

The bulk energy of a nematic LC in the absence of bounding surfaces and external actions is degenerated with respect to rotations of the nematic as whole [1]. In most cases an anisotropic surface bounding the LC lifts the degeneration producing a predominant orientation of the LC molecules on the interface. This predominant direction is called "easy axis". The orientation set by the interface propagates through the bulk. Even if a solid substrate is amorphous the degeneration is lost when the LC comes into a contact with such a substrate. In most practical cases LC molecules are strongly attached to the solid surfaces by forces of different nature. Since the atoms or molecules of the substrates are not mobile the LC director becomes fixed on the surface. This phenomena is called "surface memory effect" [68]. On contact the initial random orientation is memorized on the surface, mostly by adsorption of LC molecules [89]. The adsorbed layer behaves as new, strongly anisotropic substrate. The nematic does not suffer surface memory effect if the bounding surfaces are either liquid or gas. A thin LC film placed on isotropic immiscible liquid exhibit degenerated alignment on both interfaces with liquid and air. In many experimental situations the degenerated azimuthal anchoring conditions are required or are preferable. Several devices based on the degenerated nematic alignment were proposed [79-82]. However liquid and gas interfaces are not acceptable for commercial applications: the substrates must be necessarily rigid. The solution is to cover a solid substrate by a liquid film. Because of partial wetting the straightforward application of liquid on a solid substrate is ruled out. To avoid this problem we have deposited a thin (less than 1μm) liquid layer on a glass substrate by the condensation of evaporated glycerol. The resulting anchoring is azimuthally degenerated but appears to be not stable in time. To remove the anchoring memory one has to avoid the adsorption of the of LC for example by saturation the surface by some "passivation" layer [65]. Another possibility is to cover the substrate with highly flexible long polymer chains [64]. Brayan-Brown [90] et al. have shown that doping the LC with some impurities one can prepare the substrates with azimuthally degenerated anchoring conditions.

In our experiment the glass substrates were spin coated by one of two epoxy glue components. Nematic 5CB placed between such a substrates produces perfect degenerated planar alignment. The typical texture of a nematic with degenerated azimuthal anchoring conditions is so called Shlieren texture shown in Fig . 3. Two types of defects are seen in this figure: defects with 2 and 4 black brushes. The defects with 2 brushes correspond to the topological charge $s=\pm 1/2$ and the defects with 4 brushes have charge $s=\pm 1$. The texture (Fig. 3a) does not changes upon heating up to the temperature $T_a=36.85^o$ which is well separated from the temperature transition to the isotropic phase ($T_c=37.5^oC$). At $T= T_a$ new defects, a walls (shown by arrows in Fig.3 (b,c), 4 appear attached to each $s=1/2$ defect, while the $s=\pm 1$ defects do not suffer such a transformation. This is a direct indication that at the temperatures

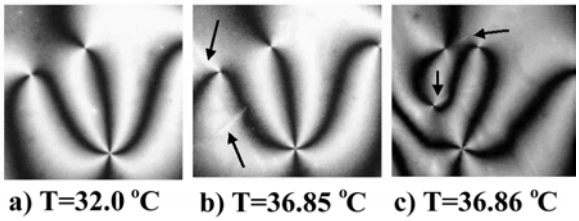

Fig. 3 Shliren texture a) before and b), c) after the anchoring transition.

$T > T_a$ the pretilt angle becomes nonzero. Indeed, this can be understood analyzing the topology of the director field around disclinations for planar and tilted alignment. The distributions of the director around the cores of s=+1/2 and s=+1 defects when the director is oriented parallel to the substrates are shown in Fig. 5a. Fig. 5b shows corresponding distributions for nonzero pretilt angle θ. It is seen that for +1 defects director orientation smoothly changes around the defect core either for zero and nonzero pretilt angle. However for +1/2 defects going along the contour drawn around the defect core we find that when we make full turn and come to the starting point, the director makes only a half of turn. As a result the director characterized by the pretilt angle $+\theta$ meets own mirror image with the pretilt angle $-\theta$ everywhere along a plane shown by a solid line in Fig. 5b. This is a new defect, the wall appearing only for nonzero pretilt angle. For exactly planar condition the wall does not exist because **n**=–**n**. Therefore observing the nematic textures one can detect the point of the anchoring transition. We notice that this observations are quit simple in their experimental realization, while the detection of the anchoring transition by other techniques is rather difficult and often ambiguous.

4. Determination of nematic polar anchoring from retardation versus voltage measurements

The results discussed in this section were obtained in collaboration with O.Lavrentovich, S.Shiyanovskii and R.Polak [31,37].

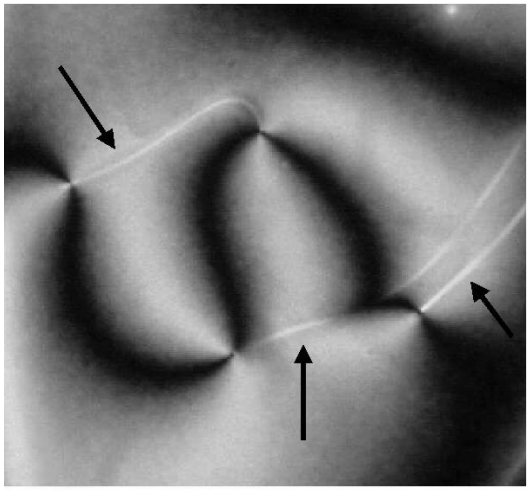

Fig. 4 Wall attached to s=1/2 defects appear after the anchoring transition

The surface orients a nematic liquid crystal director **n** along a particular orientation, called 'the easy axis'. External torques deviate **n** from its easy axis. The energetic cost of this deviation is usually characterized by an anchoring coefficient W. A variety of techniques have been developed to determine W [17-37], most of which test elastic deformations created by an external field. The most commonly used, especially for strongly anchoring cells of industrial interest, is the so-called 'high-electric-field' (HEF) technique [91] developed by Yokoyama and van Sprang [92]. It requires simultaneous measurements of the capacitance C and the optical phase retardation R of a nematic cell as a function of applied voltage V. For any value of the pretilt angle we found

$$R = A/CV - B/W \qquad (4.1),$$

where A is constant, $B = 4\pi K_1 \Delta n(1+\kappa \sin^2\theta_p)/\lambda$, K_1 and K_3 are splay and bend elastic constants, Δn is the bi-refringence, $\kappa = (K_3 - K_1)/K_1$, λ is the wave length of light, θ_p is the pretilt angle. W is determined by a simple linear fit of the data plotted in the form R vs. $1/CV$ over some voltage window $(V_{\min}, V_{\max})$ which is well above the Frederiks threshold. The resulting W is only weakly dependent on the nematic bulk

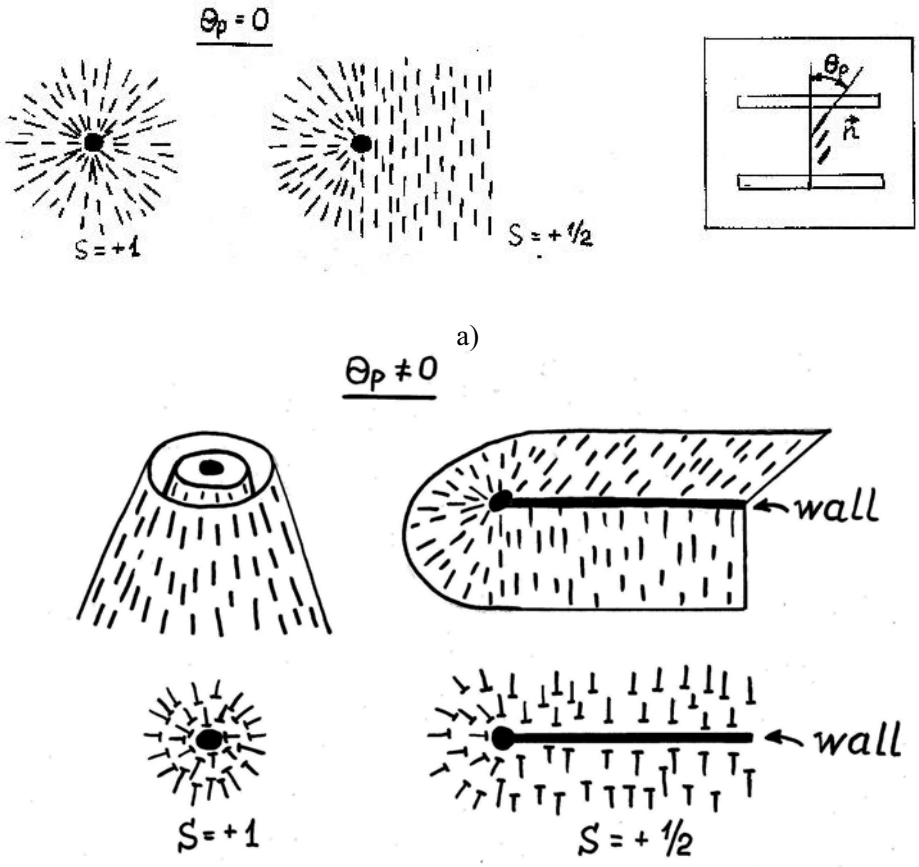

Fig. 5 The distributions of the director around the cores of *s*=+1/2 and *s*=+1 defects when the director is oriented a) parallel to the substrates, b) at nonzero pretilt angle θ.

properties and does not require an accurate knowledge of the cell thickness.

In the work [31], we seek to simplify the HEF technique by eliminating the measurement of the capacitance. The measurement of capacitance can be complicated since it requires patterned electrodes, as well as uniform cell thickness over a large area. Recently, Sun and Yokoyama suggested to overcome the difficulties by adding a small capacitance C_0, in series with the liquid crystal cell and to approximate the dependence R vs. $1/CV$ by a dependence R vs. $1/C_0V$ [93].

We have analyzed theoretically the response of the cell with a finite W to the applied field and show that this response can be completely characterized by the functional dependence R vs. V without any additional capacitors in the circuit or any assumptions about the capacitance of the cell. This approach is made possible by deriving an equation for the cell capacitance as a function of applied voltage:

$$CV = \varepsilon_0\varepsilon_{\|}S\,(V - a)/\,Qd \qquad (4.2),$$

where ε_0 is the dielectric permittivity of vacuum, $\varepsilon_{\|}$ is the dielectric permittivity along the director, S is the electrode area, *a*nd Q are parameters that are known functions of the material parameters. Their view can be found in our paper [37]. Equation (4.2) is valid over the same voltage range $(V_{\min}, V_{\max})$ as eq.(4.1). Substituting eq.(4.2) into eq.(4.1), we have the final equation to determine W:

$$R(V\text{-}a) = A_1 - B(V - a)/\,W \qquad (4.3)$$

Using the equation (4.2) in place of the measurement of capacitance, W can be determined by a simple linear fit of the

experimental dependence R vs. V according to eq.(4.3) .

A liquid crystal cell was assembled from substrates coated with a Nissan PI2555 alignment layer. First, indium tin oxide was patterned on the glass substrate to create electrodes. Second, the alignment layer on the glass was prepared by spincoating a 1:4 solution of Nissan polyimide PI2555 in the solvent HD MicroSystemsT9039 onto the substrates, baking for 1 hour at 275°C, and mechanical rubbing. Two substrates were assembled into a cell such that the rubbing directions at the plates were antiparallel. The cell gap fixed by Mylar strips was measured to be 27μm by an interference method. The optical phase retardation of the empty cell was measured to be 0.8° by the Senarmont technique.

The cell was filled with the liquid crystal 4-n-pentyl-4'-cyanobiphenyl 5CB (EM Industries). The properties of 5CB at 23 °C are as follows: K_1=6.65×10^{-12} N and K_3=8.95×10^{-12} N [94]; n_e=1.717, n_o=1.530, measured in the laboratory. To assure the most accurate implication of the experimental techniques, we measured $\varepsilon_\perp$=8.0 and $\varepsilon_\parallel$=19.5 before and after the measurement of optical retardation and capacitance. The pretilt angle of the cell was determined to be 3° by the magnetic null method [15]. All measurements were performed at 23°C.

To determine W using the HEF technique, the cell's capacitance and optical phase retardation must be measured as a function of applied voltage. Before running the experiment, the capacitance of the cell was measured using a Schlumberger SI1260 Impedance Analyzer. This serves as an experimental check of the bulk properties of the liquid crystal through determination of the threshold voltage, as well as an accurate measure of the capacitance. Leads are then attached to the cell, and it is placed in the experimental setup for the determination of anchoring. The cell is driven by a Stanford Research Systems Model DS345 function generator amplified by a Krohn-Hite Model 7600 Wide Band Amplifier. The 60 kHz sinusoidal potential is routed into a cell and a 30 kΩ resistor in series, and the potential drop across the resistor is measured. The voltage drop across the resistor is considered when determining the voltage across the cell. Since the resistance of the cells used was larger than 3 MΩ, and, thus, gave negligible contributions to the total impedance, the capacitance of the cell can be determined. Since the leads to the cell also add a capacitance, the results of this experiment are compared with the capacitance measured with the Schlumberger SI 1260 Impedance Analyzer, with the appropriate constant subtracted off of the former results. This gives C with an uncertainty of 1 pF.

The optical phase retardation of the liquid crystal cell is determined using the Senarmont technique with a low power He-Ne laser. Linearly polarized light at 45° with the rubbing direction impinges on the sample. The light emerging from the sample is elliptically polarized and transformed back into linearly polarized light by a quarter wave plate. The angle of the linearly polarized light was determined by rotating the analyzer to determine the point of extinction. The absolute uncertainty in the measured phase retardation is 0.5°.

Figure 6 shows the plot of RCV against CV for the cell. The contribution due to the retardation from the cell's substrates is subtracted off. By performing a linear fit from V_{min}=6V_{th} =4.3 V to V_{max} =25 V, eq.(4.1) yields W=2.3±0.3×10^{-4} J/m^2. The uncertainty quoted here reflects only uncertainties in the measured parameters. The possibility of systematic errors affecting the 'high-electric-field' technique is discussed below.

Figure 7 shows the plot of $R(V-\overline{V})$ and CV vs. $(V-\overline{V})$ for the same cell. Note that the dependence of CV on $(V-\overline{V})$ is linear with a zero intercept, in agreement with eq.(10). For

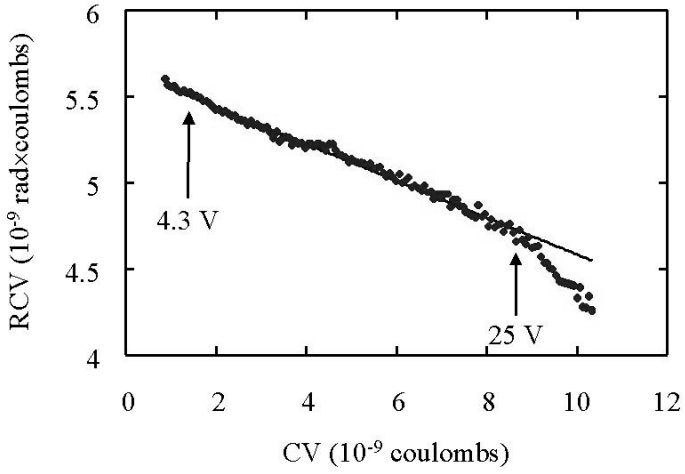

Fig. 6 Plot of *RCV* against *CV* for the same cell as in Fig. 7.

5CB in a cell with 3° pretilt, α=0.828 and $\overline{V}$ =0.39 V. With this result and fitting the experimental data from V_{min}=4.3 V to V_{max}=25 V, by eq.(4.3) yields W=2.5±0.3×10^{-4} J/m^2. The accuracy of $\overline{V}$ has a small effect on the resultant W.

We demonstrated a way to significantly simplify the determination of W by the high-electric-field technique. One should bear in mind, however, that both RV and the standard HEF technique are equally vulnerable to in-plane inhomogeneities of tested cells. Note that the theoretical models in both cases are based on one-dimensional picture of director distortions. In real cells, the in-plane inhomogeneities (e.g., variations of the easy axis and the associated anchoring potential) lead to significant deviations from the ideal theoretical response of the cell. The analysis of these deviations we performed in [37].

The analysis of current literature makes it clear that anchoring strength data may differ by two to three orders of magnitude when measured by different groups, even for the same pair of liquid crystal and substrate. We have shown that the problem is not in the lack of diligence on the part of experimentalists, but rather in the intrinsic complexity of liquid crystal behavior at the interface. We demonstrated that in many cases both techniques cannot provide meaningful values of anchoring strength: the fit

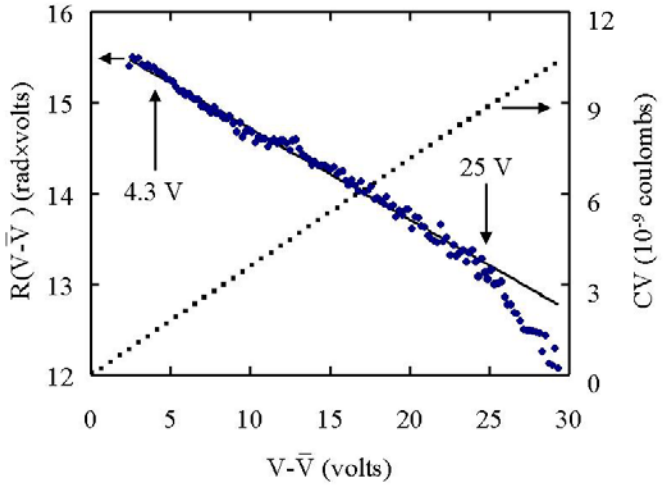

Fig. 7 Plot of $R(V-\overline{V})$ and *CV* vs. $(V-\overline{V})$ for the same cell asd in Fig. 6.

of the experimental data can produce practically any value of W, including the negative ones, within the allowed fitting region. Analysis reveals that the measured dependencies such as R vs 1/CV, measured for real cells, often do not follow the predictions of the theoretical model on which the YeS technique is based. The experimentally measured plots RCV vs. CV obtained in the experiments are schematically shown in Fig 8. One source of these discrepancies is that, in real cells the director orientation and anchoring strength are not uniform in the plane of the cell, while theory assumes strict uniformity. The problem is especially pronounced for freshly prepared cells and cells with etched electrodes needed in the YvS technique. In contrast the RV technique does not require etched electrodes and strongly enhances the reliability of W measurements. We also found that the old cells follow the predictions of the theory even if being freshly prepared they produced the negative W. The unphysical results for W originate from the in-plane director inhomogeneity. These inhomogeneity might be induced by the profile of rubbed surface substrates. For old substrates this profile is spontaneously smoothed out in time: polymer chains move as reptiles to decrease the stress produced by rubbing. This process is very slow in time and might continue several month or even years. The director surface inhomogeneity were tested in [37] by the Senarmont technique. Studying the extinction of the cell under the electric field in the Senarmont setup we found that there is no position of the analyzer for which the transmittance becomes zero. The residual transmittance T_r is a function of voltage. Analyzing the possible sources of T_r we concluded that the residual transmittance results from in-plane director inhomogeneity.

One more evidence of the in-plane surface director inhomogeneity comes from the conoscopic studies of the cell under the electric field. The experimentally observed conoscopic patterns essentially differ from the computer

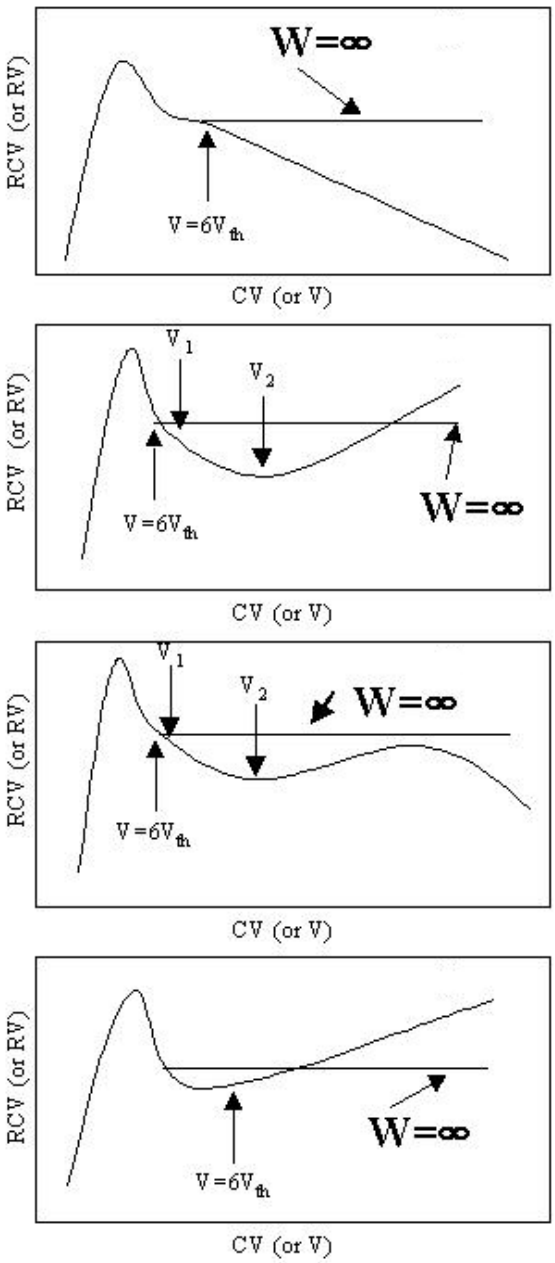

Fig. 8 Schematical representation of experimentally measured plots RCV vs. CV.

simulated figures obtained in the assumption of the uniform in-plane director distributions. These studies will be published in a forthcoming paper. Here we demonstrate a conoscopic pattern obtained at the voltage V=76V (Fig. 9). It is seen that the isogyres and the rubbing direction are located in different quadrants. Simple consideration shows that in the absence of the in-plane inhomogeneity the optic axis should remain in the plane perpendicular to the substrates and parallel to the rubbing direction **R**.

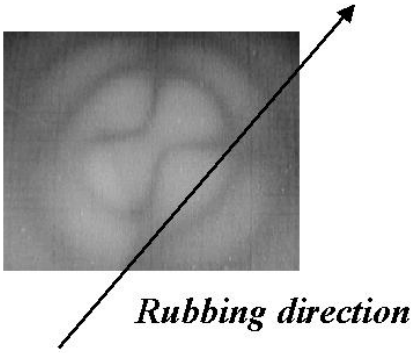

Fig. 9 Conoscopic pattern of planar cell at the voltage 76V.

As a result the cusps of the isogyre lines which represent the exits of the optic axis at the surface should be located on the line representing the rubbing direction.

5. Optical conoscopy for distorted nematics.

Conoscopy as an optical characterization technique being quite simple in its experimental realization, in fact replaces many procedures which have to be performed to probe the light propagation in a crystal at different directions. Sending a diverged light beam on the crystal which is placed between crossed polarizers one obtains an interference pattern (conoscopic figure) usually composed by two sets of lines: isogyres and isochromes. Analyzing the conoscopic figure several important crystal characteristics (type of crystal (uniaxial or biaxial), optical sign, orientation of the optical axis (axes), presence and sign of gyrotropy, birefringence value) can be easily determined following simple procedures well described in literature (see for example [38,39,95,96]). The analysis of the conoscopic pattern is based on the theory of light propagation in a crystal at different directions [39]. Although in principal the light propagation in crystals is well understood, the analysis of the conoscopic patterns is not always trivial. This especially concerns to the situations when a given conoscopic pattern results from the light interference in more than one crystal plates or when the crystal is distorted. In these complicated cases the isochrome and isogyre equations are of transcendental type and not always can be easily transformed to the equations of second order lines (circle, ellipse or hyperbola). As a matter of fact even in the simplest case of an uniform uniaxial crystal one has to use an approximation expanding complicated functions by series. The approximation procedure is quite laborious and requires careful selecting of important terms according to their weights and proving the series truncation. In most practical cases the fine structure of the conoscopic pattern is lost after the simplifications.

Another way to analyze complicated functions describing a conoscopic pattern is to generate their so-called Density Plot using an advanced programming software as for example Mathematica or Maple [13]. These programming packages allow to work with exact expressions without approximations. The Density Plot package maps values of function $f(x,y)$ as points of different brightness such that $f(x,y)=0$ is represented by a black dot in a given point (x,y), the highest f value corresponds to a white dot and the intermediate values are plotted as dots of corresponding gray levels. The Density Plot of the calculated light intensity function $I(x,y)$ for the conoscopic pattern look one to one as corresponding experimental conoscopic figures. In our previous paper [13] we proposed an algorithm for computer simulation of conoscopic patterns for distorted uniaxial nematics. We extend this approach to the simulation of the conoscopic pattern for gyrotropic uniaxial crystals in our paper [97].

The observation of the conoscopic figures precedes to any optical investigation of a newly grown (or obtained in some other way) crystalline specimen. The conoscopic figure of a thick (~ 5mm) solid crystal can be easily obtained on a screen simply by laser illumination of the crystal placed between crossed polarizers. Although there is no

principal difference between the conoscopic figures of conventional solid crystals and liquid crystals (LC's), the conoscopy is used for characterization of LC's not very often. First of all the main information on the structure of a LC sample can be obtained by the direct observation of its texture under the polarization microscope. There are some technical (but not principal) difficulties in the conoscopy of LC's. Usually LC samples are thinner than few tens of microns. As a result because of limited aperture only the isogyres and few isochromes can be observed on the screen. Only the isogyres usually are observed under the polarization microscope, while isochromes are out of the microscope field. Nevertheless in some special cases, as for example when it is necessary to establish whether the LC is uniaxial or biaxial the conoscopy is used [98-104]. The experimental observation of the conoscopic figures of the nematic cell under external field was used long time ago for the demonstration of the field reorientation effect in nematics [105]. The conoscopic figure of a twisted cell was analyzed theoretically by Maugin [106], and later Cladis [107] has used the analysis of the conoscopic picture for the measurement of the nematic twist elastic constant. The computation of the conoscopic figures of homogeneous LC's and the analysis of the influence of the lens aberrations were performed in [108]. It is also worth to notice that the crystal rotation technique (CRT) [14] for the measurement of the pretilt angle of the director in a nematic cell, based on the analysis of the angle dependence of the transmittance of the cell between crossed polarizers, is nothing else but the analysis of one-dimensional crossection of the conoscopic pattern. The conoscopy in its conventional application is developed mostly for the characterization of single crystals. We did not find in literature the description of the conoscopic figures calculation for distorted liquid crystals.

Fig 10. shows computer simulated pictures for the cells containing different types of hidden deformations, which are schematically shown under each conoscopic pattern. Fig. 10a is the conoscopic pattern for the hybrid cell. The hidden deformation shown in Fig. 10b for a quasi-homeotropic cell is visualized as splitting of the isogyres. The cusps of the isogyres indicate the exit point for the optical axis at the substrate surfaces. The director distribution from Fig. 10c appears when the upper substrate of a homeotropic cell is pushed down or for quasy homeotropic cell with parallel rubbing (not anti-parallel which produces slightly tilted uniform director distribution). This conoscopic pattern looks simillar to that for a biaxial crystal. Therefore the conoscopic pattern for a quasi homeotropic cell with parallel rubbing can be misidentified as a signature of biaxiality. It is seen that the cell with hidden twist deformation

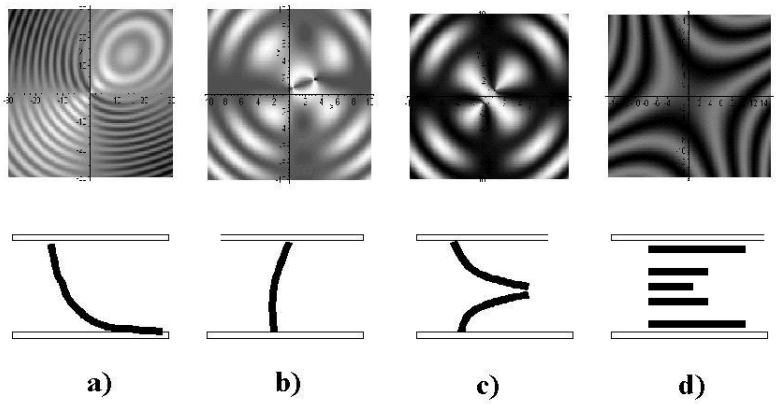

Fig. 10 Computer simulated pictures for the cells containing different types of hidden deformations, which are schematically shown under each conoscopic pattern.

(Fig. 10c) produces a conoscopic pattern that is rotated with respect to the uniform planar cell. We point out that all the deformations shown in Fig. 10 are hidden and cannot be observed with the polarization microscope, while the conoscopy can be successfully used for their detection. Detailed consideration of this problem can be found in [13].

6. Optical study of a lyotropic chromonic nematic

Optical characterization of light absorbing distorted LCs is in general much complicated that it is for a single solid crystal. In a distorted LC cell the material parameters describing the light propagation are coordinate-dependent. Nevertheless the characterization procedures developed for the solid single crystals can be adopted to characterize LC cells. To facilitate the illustration of the characterization for distorted light absorbing nematics we recall shortly the principles of optics for light absorbing crystals.

The description of light propagation in absorbing crystal is based on the Maxwell's equations in which the dielectric permittivity ε_{ij} is a complex tensor [38,39]. Substituting the material constrain equations in the Maxwell's equations one obtains the equations for the light propagating in the crystal along the *Z*-axis of a laboratory coordinate system in a form:

$$[(1/N^2)-t_{11}]D_x + t_{12}D_y = 0$$
$$[(1/N^2)-t_{22}]D_y + t_{12}D_x = 0 \qquad (6.1),$$

where N is the complex refractive index, D_x and D_y are components of the dielectric displacement vector, $t_{ij} = \varepsilon^{-1}_{ij}$ *is* the complex inverse dielectric permittivity tensor such that $t_{ij} = t_{ji}$. Excluding D_x and D_y from the system of equations (6.1) one obtains so-called Fresnel's equation

$$[(1/N^2)-t_{11}]\,[(1/N^2)-t_{22}] + (t_{12})^2 = 0 \qquad (6.2)$$

Two solutions of equation (6.2) are of the form :

$$(1/N^2)_{\pm} = (1/2)\,[t_{11}+t_{22} \pm \{(t_{11}-t_{22})^2+4(t_{12})^2\}^{1/2}] \qquad (6.3)$$

It is known that any real tensor of second rank can be reduced to a diagonal form. The tensor can be reduced to the diagonal form by the rotation for example around its *3*-axis. However the tensor $t_{ij} = t'_{ij} + i\,t''_{ij}$ is a complex one. Further we denote components of a tensor which is in its diagonal form by a capital letter (T_{ij} for the tensor t_{ij}); the letter with the signs ' or " denote a real and imaginary parts of a complex tensor, respectively. For uniaxial crystals the principal axes of t'_{ij} and t''_{ij} tensors coincide. Hence for an uniaxial crystal rotating simultaneously the tensors t'_{ij} and t''_{ij} one can reduce the tensor t_{ij} to its diagonal form with T_{12} =0. If the crystal is biaxial the principal axes of the tensors t'_{ij} and t''_{ij} do not coincide. We reduce the real part t'_{ij} to its diagonal form rotating t'_{ij} around its axis 3. If the crystal is of the lowest symmetry the principal axes of the tensor t''_{ij} do not coincide with the axes of the tensor t'_{ij}. Then the 3-axis of the tensor t'_{ij} is not a principal axis of the tensor t''_{ij} . The rotation of the t'_{ij} tensor around its 3-axis is accompanied by the simultaneous rotation of the tensor t''_{ij} around a non-principal direction. As a result $T'_{12}=T'_{13}=T'_{23}=0$ while T''_{12} , T''_{13} , T''_{23} are nonzero.

The view of the components t_{11}, t_{22}, t_{12} from the eqs. 6.1-6.3 depends on the representation of orientation of the (*1,2,3)* crystal coordinate system with respect to the (*X,Y,Z)* laboratory coordinate system. In crystallography the axes *1,2,3* are attached to symmetry elements of crystal. For example, the orthorhombic crystals exhibit three mutually perpendicular 2-fold symmetry axes. The coordinate axes *1,2,3* of such a crystal are directed along the 2-fold symmetry axes. The *1,2,3* axes are also principal axes of the tensor t'_{ij} . The directions of the *1,2,3* axes are called the principal crystal directions. The orientation of the coordinate system *(1,2,3)* with respect to the laboratory coordinate system (*X,Y,Z*) can be described via three consequent elementary rotations. Three Euler angles θ, β, γ unambiguously characterize these rotations. The

direct cosines of new coordinate system with respect to the old one can be found by the multiplication of the matrices of elementary rotations (see [109]). There are 12 systems of the Euler angles. In practice the choice of the Euler angle system is governed by the geometry of a studied problem. Since usually in the experiment the studied crystal is rotated around the light wave vector, two angles are of the interest: polar angle and azimuth of principal crystal directions. Therefore, it is convenient to choose such Euler angle system for which two of three Euler angles are spherical coordinates of a principal crystal direction. Let the Euler angles θ and γ be the polar angle and azimuth of 3-axis of the tensor T'_{ij} in the (X,Y,Z) coordinate system. The direct cosines matrix of this Euler angle system is the matrix $A_{32} = A_3(\gamma)\, A_2(\theta)\, A_3(\beta)$, a product of three elementary rotation matrices. First the system (X,Y,Z) is rotated around the Z-axis on the angle γ, such that (X,Y,Z) transforms into $(1b,2b,3b)$ with $3b$ being directed along Z. Then $(1b,2b,3b)$ transforms into $(1a,2a,3a)$ by the rotation of $(1b,2b,3b)$ on the angle θ around $2b$, i.e. the axis $2a$ coincides with the axis $2b$. And finally $(1a,2a,3a)$ transforms into $(1,2,3)$ by the rotation of $(1a,2a,3a)$ on the angle β around $3a$, i.e. $3a$ is along 3. We recall that we have chosen the Z-axis along the light wave vector. The X-axis is chosen along the polarization of incident light. In the (X,Y,Z) coordinate system

$$t_{11} - t_{22} = a\cos2\gamma + b\sin2\gamma; \quad (6.4a)$$

$$2t_{12} = b\cos2\gamma - a\sin2\gamma; \quad (6.4b)$$

$$t_{11} + t_{22} = 2c - a, \quad (6.4c),$$

where

$$a = T_{11}\{\sin^2\beta - \cos^2\beta\cos^2\theta\} + T_{22}\{\cos^2\beta - \cos^2\theta\sin^2\beta\} - T_{33}\sin^2\theta + T_{12}\sin2\beta(1+\cos^2\theta) + \{T_{23}\sin\beta - T_{13}\cos\beta\}\sin2\theta; \quad (6.4d)$$

$$b = \{(T_{11} - T_{22})\sin2\beta + 2T_{12}\cos2\beta\}\cos\theta + 2\{T_{13}\sin\beta + T_{13}\cos\beta\}\sin\theta; \quad (6.4e)$$

$$c = T_{11}\sin^2\beta + T_{22}\cos^2\beta + T_{12}\sin2\beta; \quad (6.4f)$$

Then the refractive indices of the eigenwaves are of the form:

$$(1/N^2)_{\pm} = (1/2)\,[2c - a \pm \{a^2+b^2\}^{1/2}] \quad (6.5).$$

The polarization state of eigenwaves can be deduced from the ratio $r=D_y/D_x$. The azimuth χ and ellipticity s (or ellipticity angle ε) of the eigenwaves can be calculated as:

$$tg2\chi = 2Re[(r)/(1-|r|^2)], \quad (6.6)$$

$$s=\sin2\varepsilon = -2i\,Im[(r)/(1+|r|^2)] \quad (6.7).$$

From the equations system (6.1) we have

$$r=((1/N^2)-t_{11}) / t_{12} \quad \text{or} \quad 1/r = ((1/N^2)-t_{22}) / t_{12} \quad (6.8)$$

Substituting (6.5) in (6.8) we find

$$r_+ = -1/r_- \quad (6.9a)$$

$$r_+ = [-a\sin(2\gamma) - b\cos(2\gamma) + \{a^2+b^2\}^{1/2}] / (b\cos2\gamma - a\sin2\gamma) \quad (6.9b)$$

First equation of the system (6.9) shows that the eigenwaves are orthogonal. For weak light absorption the parameter b can be considered to be imaginary, i.e. $b=ib''$ and the parameter a to be real, i.e. $a=a'$. Then substituting eq.(6.9b) into equation (6.7) we find

$$s=s_+=s_-= b''/a' \quad (6.10)$$

The equation (6.10) shows that in a general case the eigenwaves in the absorbing biaxial crystal are elliptically polarized and have equal ellipticities. The ellipses of the eigenwaves are orthogonal. The parameters a, b, c are functions of polar angles θ, β and do not depend on the azimuth angle γ. Therefore the refractive indices of the eigenwaves and their ellipticity are functions of the angles between the light wave vector and the principal crystal directions and do not depend on the azimuth of crystal principal directions. For transparent crystals $b''=0$. Therefore the eigenwaves for a transparent biaxial crystal are linearly polarized. From eq.(6.5) one can see that for a light absorbing crystal $N_- = N_+$ when

$$a^2 + b^2 = 0 \quad (6.11a)$$

or in the assumption of weak absorption when

$$(a')^2 - (b'')^2 = 0 \quad (6.11b).$$

Eqs. (6.11b) defines the orientation of the optical axes of absorbing crystal with respect to

the principal crystal directions. Substituting eq. (6.11b) into eq. (6.10) we obtain s=1, i.e. we find that the eigenwaves are circularly polarized if the light propagates along the directions satisfying the condition (6.11b). For this reason the 4 directions defined by eq. 6.11b are termed as circular axes of absorbing crystal.

For a light absorbing crystal of the orthorhombic and monoclinic symmetry $T'_{13}=T'_{23}= T''_{13}=T''_{23}= T'_{12}= T'_{13}=0$ while $T''_{12} \neq 0$. From eqs. (6.4d), (6.4e), (6.9b) one can find that when $\theta=0$ or $\pi/2$ the parameter r becomes purely real and as a result $s=0$. In other words the eigenwaves are linearly polarized if the light wave vector is perpendicular to the 2-fold symmetry axes.

The intensity of the monochromatic linearly polarized light passed through the biaxial absorbing crystals can be found using the method of eigenwaves superposition. Following the approach described in [39] for the light transmittance (normalized light intensity I/I_0) we obtain:

$$T= e^{-(4\pi/\lambda)\kappa d} [((1+s^2) /(1-s^2))^2 \{ch(\delta) - \cos(2\gamma) sh (\delta)\} + (2s /(1-s^2)) \sin (2\gamma) \sin(\Delta) - (2s /(1-s^2))^2 \cos(\Delta)] \quad (6.12)$$

where, $\kappa=(\kappa_1+\kappa_2)/2$, κ_1 and κ_2 are absorbing coefficients for two eigenwaves, d is the thickness of the crystal, $\delta=(2\pi/\lambda)(\kappa_1-\kappa_2)$, γ is the azimuth angle of the incident light polarization with respect to the principal crystal directions, s is the ellipticity of the eigenwaves. For uniaxial absorbing and nongyrotropic transparent crystals s=0. For biaxial absorbing crystals s takes a value between 0 and 1 depending on the crystal orientation with respect to the wave vector of the eigenwaves. The ellipticity s is equal to 1 along the circular axes and decreases very quickly apart from these directions. The light propagation along the circular axes and in their vicinity was considered in [6]. When light passes along the circular axis $\delta=\Delta=0$.

As it follows from the expression (6.12) there is a remarkable difference between the transmittance of uniaxial and biaxial absorbing crystals. Let us introduce a parameter

$$\Delta T = T_{45} - (T_{90}+T_0)/2,$$

where T_0 , T_{45}, T_{90} are the transmittancies at $\gamma=0^o$, 45^o and 90^o, respectively.

For an uniaxial crystal s=0 and for all wavelength we have:

$$\Delta T = 0 \quad (6.13),$$

While for a biaxial crystals:

$$\Delta T = e^{-(4\pi/\lambda)\kappa d} (2s /(1-s^2)) \sin\Delta \quad (6.14)$$

Experimental study of the light transmittance for a lyotropic chromonematic. The relations (6.13) and (6.14) can be used as a test for biaxiality. Eq. 3 shows that for a biaxial crystal ΔT is an oscillating function of phase retardation. One can change the phase retardation Δ changing the light wave length λ. Plotting the function $\Delta T(\lambda)$ calculated from

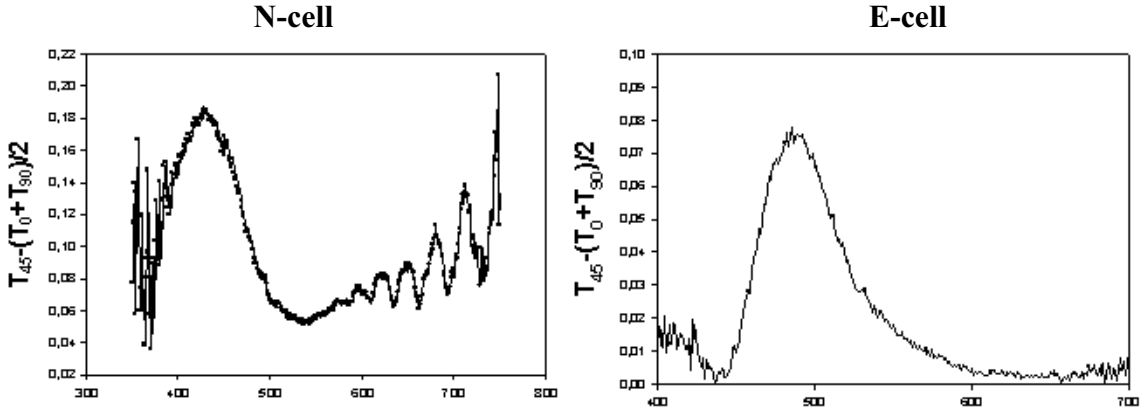

Fig. 11 $\Delta T(\lambda)$ for N-, and E- cells of the light absorbing lyotropic nematic.

experimentally obtained spectra one can distinguish between the uniaxial and biaxial crystals. Figures 11 show $\Delta T(\lambda)$ for so called N-, and E–cells of the light absorbing lyotropic nematic. Chromonics are lyotropic liquid crystals formed by the dispersion of orientationally ordered anisotropic aggregates of dye molecules in a solvent. The cells differ by the orientation of the nematic with respect to the substrates. The details will be published in a forthcoming paper. It is seen that these cells have similar behavior of the $\Delta T(\lambda)$ envelope. However they differ by the presence of the oscillations for N-cell. The nonzero dependence $\Delta T(\lambda)$ for these three cells as well as oscillations for N-cells are the signatures of the biaxiality of the studied chromonematic. According to (6.14) the envelope of the $\Delta T(\lambda)$ line is defined by the factor $e^{-(2\pi/\lambda)\kappa d}(2s/(1-s^2))$ and its oscillating character is dictated by $sin\Delta$. Although the E-cell displays the high azimuth dependence of the transmittance similarly as it is for the N-cell the oscillations are not observed for E-cell. This fact indicates that the direction of light propagation in the E-cell corresponds to $s=0$. As it was mentioned above the light ellipticity is zero when the 2–fold symmetry axis of the crystal is perpendicular to the light wave vector. We believe that the absence of the oscillations for E–cell results from the orientation at which the 2–fold symmetry axis is parallel to the substrates. Therefore the absence of the oscillations on the dependence $\Delta T(\lambda)$ for E-cell shows that for this cell the ***n***-director is parallel (or almost parallel) to the substrates. The presence of the oscillations for the N-cell indicates that $s\neq 0$, i.e. that for these two cells ***n*** is tilted with respect to the substrates.

One can estimate the Δn value from the oscilation period in Fig 11. We found Δn = 0.1. Other possible mechanisms of the existence of $\Delta T(\lambda)$ oscillations can not produce the periodicity about 28nm. Indeed, the oscillations can not result from the reflection interference on a cell gap. For the cell gap with refractive inex n about 1.5 and d=75μm we find the oscillations with the wave length 4nm (compare to 28nm observed on ΔT(λ)). Moreover they are not produced by the glass substrates with the thickness about 2mm. Such oscillations could result from the interference on a 2.5μm hypothetical layer with the refractive index n=1.5. However there is no reason to expect any layer of this thickness inside the cell.

Polarized microscopy observations. It is known that the nematic texture observed under the polarization microscope visualizes director field distortions and defects. In nonabsorbing nematics not all the distortions can be recognized and unambiguously characterized under the polarization microscope. For nonabsorbing nematic the nontrivial texture is produced only by singular defects and in-plane distortions, while smooth distortions in the plane perpendicular to the substrates are hidden. Singular defects are seen even without analyzer, whereas out-of-plane distortions can not be distinguished even from uniform non-homeotropic director field. In absorbing nematics the textures are more informative. The texture is colored even without analyzer. For uniaxial light absorbing nematics two distinctive colors or their mixture can be observed without analyzer.

When a ray of unpolarized (ordinary) light falls on a dichroic uniaxial crystal, any given wavelength will be absorbed differently according which plane it is vibrating in, except along the optic axis for which there is no distinction between an ordinary ray and extraordinary ray. Thus, the uniaxial dichroic crystal will appear to have one color in the direction of the optic axis and a different one at the other angles. The mixture of these two distinctive colors can be expected for liquid crystals where a light ray propagating across the sample crosses the optic axis at different angles. Indeed, for the unoriented thermotropic nematic

E7 doped by gentle amount of Methyl Red we have observed two distinctive yellow and red colors and their brown mixtures (yellow with red and red with yellow). Yellow color corresponds to the light propagating along the director and red one to the light polarization being parallel to the director. It is evident that the brown color is a mixture of yellow and red colors but not a distinctive principal color.

In a thick cell with untreated substrates observed without analyzer our chromonematic B27 is much reach of colors. We find three distinctive colors: yellow, red and pink as well as colors appearing by their mixing. Non of three mentioned distinctive colors can be obtained by mixing of two others. The appearance of three distinctive colors can be considered as a signature of biaxiality. Corresponding light absorption phenomenon observed in the biaxial solid crystals is called trichroizm. Defocusing the microscope we find that the distinctive colors result from the bulk but not from surface absorption. Hence, trichroizm is not induced by the surface and can be explained by bulk biaxiality.

References

1. P.G deGennes and J.Prost, The Physics of Liquid Crystals, Calendon Press, Oxford (1993).
2. L.M.Blinov and V.G.Chigrinov, Electrooptic Effects in Liquid Crystal Materials., Springer, New York (1994).
3. N.H.Hartshorn, The microscopy of Liquid crystals, Microscope Publications, London, (1974).
4. J.M.Haudin, in: G.H.Meeten (Ed.), Optical properties of Polymers, Elsevier, Essex, (1986) 167-264.
5. J.R.Bellare, H.T. Davis, W.G. Miller, L.E. Scriven, J.Colloid Interface Sci. **136** (1990) 305p.
6. W.L.Mc.Millan, Phys.Rev.A **4** (1971) 1238p.
7. W.L.Mc.Millan, Phys.Rev.A **6** (1972), 936p.
8. E.S.Lukyanchenko, V.A.Kozunov, V.I.Grigos. Adv. of. Chem. Sc. (Sov.) **54** N2 214p. (in Rissian).
9. V.N. Matveenko, E.A.Kirsanov. Surface Phenomena in Liquid Crystals. Moscow. University. Moscow. (1991) (in Rissian).
10. I.I.Smalyukh, S.V.Shiyanovskii, O.D.Lavrentovich, Chem.Phys. Lett. **336** (2001) 88-96.
11. S.V.Shiyanovskii, I.I.Smalyukh and O.D.Lavrentovich. Chemical Physics Letters **336** (2001) 88-96.
12. R. H. Webb, Confocal optical microscopy. Rep. Prog. Phys. **59** (1996) 427-471.
13. Yu.A.Nastishin, O.B.Dovgyi, O.G.Vlokh, Ukr. J. Phys. Opt. **2** (2001) 98-106.
14. Baur G., Wittwer V. and Berreman D.W. Phys. Lett. A **56** (1972) 142p.
15. T.J.Sheffer and J.Nehring, J.Appl.Phys. **48** (1977) 1783p.
16. A.Rapini and M.Popular, J.Phys. (Paris), Colloq. **30** (1969) C-4.
17. L.M. Blinov, A. Yu. Kabayenkov, and A.A.Sonin, Liq.Cryst. **5** (1989) 645p.
18. M.Kleman and Williams, Philos. Mag. **28** (1973) 275p.
19. G.Ryshenkow and M.Kleman, J. Chem Phys. **64**. (1976) 404p.
20. G.Barbero, N.V. Madhusudana and G.Durand, J.Phys. (France) Lett.. **45** (1984) L-613.
21. T. Marusiy, Yu.Reznikov, and V. Reshetnyak, Sov. Phys. JETP **64** (1986) 502p.
22. S. Naemura, Appl. Phys. Lett. **33** (1978) 1.
23. K.H.Yang andC. S.Rosenblatt, Appl. Phys. Lett. **43** (1983) 62p.
24. J.T. Gleeson and P.Palfy-Muhoray, Liq. Cryst. **5** (1989) 663p.
25. D.F. Gu, S.Urah, and C. Rosenblatt Liq. Cryst. **19** (1995) 427p.
26. S. Subacius, V.M. Pergamenshchik, and O.D.Lavrentovich, Appl. Phys. Lett. **67** (1995) 214p.
27. S. Faetti and V. Palleschi, J.Phys. (France) Lett. **45** (1984) L-313.

28. H.Yokoyama and H.A. van Sprang, J. Appl. Phys. **57** (1985) 4520p.
29. H. Yokoyama, S.Kobayashi, and H.Kamei, J.Appl. Phys. **61** (1987) 4501p.
30. H. Yokoyama, in Handbook of Liquid Crystal Research, edited by P.J. Collings and J.S. Patel (Oxford University Press., New York. 1977) 179p.
31. Yu.A.Nastishin, R.D.Polak, S.V.Shiyanovskii, and O.D.Lavrentovich, Appl. Phys. Lett. **75** (1999) 202p.
32. M. I. Barnik, L.M. Blinov, T.V.Korkishko, B.A. Umansky, and V.G.Chigrinov, Mol. Cryst. Liq. Cryst. **99** (1983) 53p.
33. O.D. Lavrentovich, V.G. Nazarenko, V.V. Sergan, and G.Durand, Phys. Rev.A **45** (1992) R6969.
34. G.Barbero and G.Durand, J.Appl. Phys. **67** (1990) 2678p.
35. H.Yokoyama, Mol. Cryst. Liq.Cryst. **165** (1988) 269p.
36. Y. Ji, J.R. Kelly, and J.L. West, Liq. Cryst. **14** (1993) 1885p.
37. Yu.A.Nastishin, R.D.Polak, S.V. Shiyanovskii, V.H.Bodnar, and O.D.Lavrentovich, J. Appl. Phys. **86**, N8 (1999) 4199-4213.
38. M.Born and E.Wolf, Principles of Optics (Pergamon, Oxford, 1980)
39. A.F. Konstantinova, B.N. Grechushnikov, B.V. Bokut, E.G. Valyashko, Optical Properties of crystals., Minsk, Navuka i tekhnika (1995). (in Russian).
40. Yu. A. Nastishin, M. Kleman, J. Malthête, and H. T. Nguyen , Eur. Phys. J. **E5** (2001) 353p.
41. L.Navailles et al., J.phys II **6** (1996) 1243p.
42. P.Kassubek, G. Meier, Mol. Cryst. Liq. Cryst. **8** (1969) 305p.
43. R.S. Pindak et al., Solid State Commun. **15** (1974) 429p.
44. R.S. Pindak et al., Phys. Rev. Lett. **32** (1974) 43p.
45. P.G.de Gennes, Solid State Commun. **10** (1972) 753p.
46. S.R.Renn, T.C. Lubensky, Phys. Rev. A **38** (1988) 2132p.
47. J.W. Goodby et al., Nature **337** (1989), 449p.
48. O.D. Lavrentovich et al., Europhys. Lett. **13** (1990) 313p.
49. K.J.Ihn et. al., Science **258** (1992) 275p.
50. N.Isaert et al. J.Phys. II **4** (1994) 1501p.
51. R.D.Kamien, T.C.Lubensky J. Phys. II **3** (1993) 2131p.
52. M.H.L. Pryce et al., in Robinson C. et al., Discuss. Faraday Soc. **25** (1956) 29p.
53. J.Fridel, M.Kleman, J.Phys. (Paris) Colloq. **30** (1969) C4:43.
54. G.E.Volovik, V.P.Minyeev, Jetp Lett., **45** (1977) 1186p.
55. Y. Bouligand, F. Livolant, J. Phys. (Paris) **45** (1994) 1899p.
56. V.G.Nazarenko, A.Nych, Phys. Rev. E **60** (1999) R3495.
57. P. Sheng, Phys. Rev. Lett. **3**7 (1976) 1059p.
58. H.Mada, Sh.Kobayashi, Mol. Cryst. Liq. Cryst., **33** N1/2 (1976) 47p.
59. V.I. Sugakov, S.V. Shiyanovskii. Ukr. Phys. J. **22** N9 (1977) 1441p. (in Russian)
60. T.Moses and Y.R.Shen, Phys. Rev. Lett. **67** 15 (1991) 2033 p.
61. E.Smela and L.J.Martinez-Miranda, Liq. Cryst. **14** N6 (1993) 1877-1883.
62. P.de Schrijver, W.van Dael and J.Thoen, Liq. Cryst. **21** N5 (1996) 745-749.
63. R. Barberi and G. Durand, Phys. Rev. A **4**1 (1990) 2207p.
64. O. Ou Ramdane, Ph.Auroy, S.Forget, E.Raspaud, Ph. Martinot-Lagarde, and I. Dozov , Phys.Rev. Lett. **84** 17 (2000) 3871-3874.
65. Ph. Martinot-Lagarde et al., French Patent No. 2763145 (1997).
66. O.D.Lavrentovich, Yu.A.Nastishin, Europhys. Lett., **13** (1990) 135-141.
67. O.D. Lavrentovich and V.M.Pergamenshchik, Lett. J. Tech. Phys. (Sov.). Phys. **15** (1989) 73p. (in Russian).; Sov.Tech Phys. Lett, **15** (1989) 194p.
68. Y. Ouchi, M. B. Feller, T. Moses, and Y. R. Shen, Phys.Rev. Lett. **68** (1992) 3040p.

69. B. Jérôme, Rep. Prog. Phys. **54** (1991) 391p.
70. G. Ryschenkow and M. Kléman, J. Chem. Phys. **64** (1976) 404p.
71. M. Monkade, M. Boix, and G. Durand, Europhys. Lett. **5**. (1988) 697p.
72. B. Jérôme, P. Pieranski, and M. Boix, Europhys. Lett. **5** (1988) 693p.
73. J. Bechhoefer et al., Phys. Rev. Lett. **64** (1990) 1911p.
74. P. I. C. Teixeira and T. J. Sluckin, J. Chem. Phys. **97** (1992) 1498p.
75. J. S. Patel and H. Yokoyama, Nature (London) **362** (1993) 525p.
76. Yang-Ming Zhu et al., Phys. Rev. Lett. **72** (1994) 2573p.
77. P. Jägemalm, G. Barbero, L. Komitov, and A. Strigazzi, Phys. Lett. A **235** (1997) 621p.
78. D.Andrienko, A.Dyadusha, Yu.Kurioz, V.Reshetnyak, and Yu.Reznikov, Mol. Cryst. Liq. Cryst **321** (1998) 299-307.
79. G. Durand, Proceedings of SPIE **2949** (1996) 2.
80. I. Dozov, M. Nobili, G. Durand, , Appl. Phys. Lett. **70** (1997) 1179p.
81. I. Dozov, Ph. Martinot-Lagarde, E. Polossat, I. Lelidis, M. Giocondo and G.Durand, , Proceedings of SPIE **3015** (1997) 61.
82. Ph. Martinot-Lagarde, I. Dozov, E. Polossat, M. Giocondo, I. Lelidis, G. Durand, J. Angelé, B. Pecout and A. Boissier, , SID '97 Digest, **41** (1997).
83. K. Miyano, Phys. Rev. Lett. **43** (1979) 51p.
84. R. Lipowsky, Phys. Rev. Lett. **49** (1982) 1575p.
85. G. P. Crawford, R. Ondris-Crawford, S. Zumer, and J. W. Doane, Phys. Rev. Lett. **70** (1993) 1838p.
86. J. Xue, C. S. Jung, and M. W. Kim, Phys. Rev. Lett. **69** (1992) 474p.
87. M. P. Valignat et al., Phys. Rev. Lett. **77** (1996) 1994p.
88. O.D.Lavrentovich, V.G.Nazarenko, V.V. Sergan, and G.Durand, Phys.Rev.a **45** (1992) R6969.
89. J. Cheng and G. D. Boyd, Appl. Phys. Lett. **35** (1979) 444p.
90. G. P. Bryan-Brown, E. L. Wood, and I. C. Sage, Nature (London) **39** (1999), 338p.
91. H.Yokoyama, in Handbook of Liquid Crystal Research, edited by P.J.Collings and J.S.Patel (Oxford University Press, New York, 1997) 179p.
92. H.Yokoyama and H.A. van Sprang, J. Appl. Phys. **61** (1987) 4501p.
93. R.Sun and H.Yokoyama, presented at the 4th International unit of Material Research Society, International Conference in Asia, Chiba, Japan, September (1997) (unpublished)
94. M.J.Bradshaw, E.P.Raynes, J.D. Bunning and T.E.Faber, J.Phys. (Paris) **46** (1983) 1513p.
95. Vlokh O.G. Phenomena of spatial dispersion in parametric crystalloptics. Lviv. "Vyshcha shkola" (1984). (in Russian)
96. Romanyuk M.O. Crystalloptics. Kiev. IZMN. (1997) (in Ukrainian)
97. Yu.A.Nastishin, O.G.Vlokh, O.B.Dovgyi, Ukr. J. of Phys. Opt. **2** (2001) 133-140.
98. Yu L.J.and Saupe A., Phys. Rev. Lett. **45**, (1980) 1000p.
99. Chandrasekhar S., Nair Geetha G., Rao D. S. Shankar, Prasad S. Krishna, Praefcke K., Blunk D. Curr.Sci. **75** (1998) 1042-1046.
100. Galerne Y. and Marcerou J.P. Phys. Rev. Lett., **51** 23 (1983) 2109p.
101. Gorechka E., Chandani A.D.L., Ouchi Yu., Takezoe H., Fukuda A. Jpn. J. Appl.Phys., **29** 1 (1990) 131p.
102. Moritake H., Ozaki M., Tanigushi H., Satoh K., Yoshino K. Jpn. J. Appl.Phys., **33** Part 1 N.9B (1994) 5503p.
103. Fujikava T., Hiraoka K., Isoaki T., Kajikava K., Takezoe H., Fukuda A.. Jpn. J. Appl.Phys., **32** Part 1 No.2 (1993) 985p.
104. Natano J., Nanaki Y., Furue H., Uehara H., Saito Sh., Murashiro K. Jpn. J. Appl.Phys., **33** Part 1 No.9B (1994) 5498p.
105. Prost, J. and Gasparoux, H. C. R. Acad. Sci. Paris **C273** (1972) 335p.

106. Maughin, Bull C. Soc. Fr. Miner. **34** (1911) 71p.
107. Cladis P.E.. Phys. Rev. Lett. **31**. (1973) 1200p.
108. MacGregor A.R.. J. Opt. Soc. Am. A, vol.7, No.**3**,(1999) 337p.
109. G.A.Korn and T.M.Korn, Mathematical handbook. McGraw-Hill Book Company, New-York, 1968.